Thermal Performance of Radiant Floor Heating Systems

Concrete Slabs

Kiran Tota-Maharaj [1]*, and Blessing Oluwaseun Adeleke[2]

[1] College of Engineering and Physical Sciences, Department of Civil Engineering, School of Infrastructure & Sustainable Engineering, Aston University, Birmingham, B4 7ET, UK

[2] School of Engineering, Faculty of Computing, Engineering and Science, University of South Wales, Pontypridd, CF37 1DL, UK

*Corresponding author. Tel: +44 (0) 121 204 4296, E-mail: k.tota-maharaj@aston.ac.uk

Abstract

This paper investigated the application of recycled steel powder as an additive in concrete to increase the thermal properties of radiant floor heating systems (RFHS). The project aimed to increase the efficiencies of thermal conductivities, allowing radiant heat to produce higher energy efficient outputs for heating. Thermocouple readings measured lower temperatures with similar heating conditions as a standard mix slab due to heat transfer occurring evenly through a large surface area, thus transferring heat to the air at faster rates. The tests were completed by casting two 400×400×200mm deep slabs enclosing radiant heating pipes. Water was pumped at 40 and 60°C through the pipes. The temperature was recorded at various positions throughout the slab that would allow the multi-layered cylinder approach to analyse the rate of heat transfer, and calculate the efficiency of the heat transfer. The crushing strength of the proposed mix using steel powder replacement is shown to be reduced by 26% when a mix with 12.4% of steel powder is used. Contrary to the original hypothesis of this research, the

1 investigation found rates of heat transfer during the heating stage were 3% lower for the mix

2 containing steel powder compared to the standard mix.

3

4 **Keywords:** Energy Efficiency, Radiant Floor Heating System (RFHS), Thermal

5 Performance, Temperature Flux, Concrete Slabs, Heating Elements

6

Notation

λ	Turbulent thermal conductivity W/(K m)
q_{ra}^{out}	Heat Flux out W/m^2
q_{hw}^{in}	Heat Flux in W/m^2
ΔT	Temperature Differential
c	Specific Heat Capacity (kJ/kg ^{o}C)
$C35$	Grade Concrete strength (35 N)
k	Thermal conductivity (W/mK)
L	Length of Slab (m)
NM	Normal Mix
Q	Heat (J)
r	Radius from centre point to various sections (m)
$RFHS$	Radiant Floor Heating System
SM	Steel Mix
T	Thermodynamic temperature (K or ^{o}C)
V	Volume (m^3)
ρ	density of fluid/liquid (kg/m^3)

β Constant for distance between RFHS

h_{total} Total heat transfer coefficient (W/m^{2}K)

q_{total} Total heat flux density (W/m^2)

1.0   Introduction

The negative effect of global warming on the world and the drive to protect the environment has rapidly gathered pace over time. This is evident in the global awareness and the implementation of policies by the UK government to support the development of greenhouse gas reducing technologies. An industry that has been singled out is the space heating of buildings with renewable/low carbon heat incentives and a "future home standard". (Department for Business, 2019). This will require all residential new builds to possess higher levels of insulation capacity and the phasing out of gas heating in buildings by 2025 (Hammond, 2019). This campaign is anticipated to provide an ideal setting for radiant heating systems to be adopted as the standard heating method in new builds in the UK. As a result of the inclusion of greenhouse gas emissions of space heating in the "government priorities", there is a large amount of research going into Radiant Floor Heating systems (RFHS), a contender for the future of heating. RFHS possesses lower operating water temperature compared to radiator systems generally used in the UK, circa 40°C compared to 60°C, reducing the energy needed to heat a room. A study by Miriel et al. (2002) demonstrated the potential savings of up to 30% in applying the RFHS technology. In addition, RFHS boast a more even and comfortable heat source in a room than other forms of heating and higher compatibility with low-grade heat sources such as solar hot water and heat pumps (low-carbon heating sources). However, RFHS have two (2) notable areas for potential improvement namely:

(i)   The delay (lag time) between the switching on of the heating and room temperature increase.

(ii) Uneven surface temperature distribution of the system.

When heating a room using RFHS, there is a more considerable lag time from turning on the heating to the room temperature being changed compared to other heating methods. The reason for this is that the heat has to be transferred from the water to the pipe, then through approximately 20 to 100mm of concrete in most cases, which finally diffuses into the air. In contrast, a conventional radiator simply transfers heat through convection from the water to the radiator and then directly to the atmosphere. Most RFHS have high and low heat spots depending on location in relation to the pipe. This makes for a less comfortable environment for the occupants of the room and is a less efficient use of heating energy than would be obtained from a uniformly heated floor. Recent trends aimed at ensuring the fire resistance of structures have encouraged increased use of performance-based approaches, which are now often categorised as structural fire engineering (Cho et al., 2019). These methods attempt to use various material additives, and the actual behaviour of the three-dimensional structure is modelled at different degrees. This approach considers the realistic fire exposure scenarios, loss of some load from the ultimate to the fire limit state, actual material behaviour at elevated temperatures and interaction between various parts of the structure.

1.1   *Availability of Materials*

It was estimated that 50% of all metals used in UK manufacturing are recycled (Maxilead-Metals, 2019). However, this still leaves a significant amount of scrap metal that is not being recycled. Principally, fine powder steel, which is a costly and difficult material to recycle. In order to use the powder to create a solid metal, the powder must be initially graded to uniform sizes before sintering. Consequently, studies have found that distribution in particle size can

decrease the final mechanical and material properties (Averyanova et al., 2012, Karapatis et al., 1999). However, grading the material requires specialist machinery as the powder blinds the mesh in universal grading systems. Therefore, recycling bulkier steel waste is cheaper and more practical than sintering fine steel resulting in very small volumes being recycled into solid steel. Although the supply of fine steel powder is currently greater than demand, it is becoming a more sought-after product due to the production-scale metal powder Additive Manufacturing (AM) developed in the 2010s (Tofail et al., 2018). The demand for AM is expected to grow as it allows for "bottom-up" manufacturing layer by layer instead of conventional forging and machining. This will likely mean the uptake rate will continue to grow, leading to an increase in the manufacturing of powder steel, thus allowing for easy and affordable supply for use as an additive in concrete manufacturing, as proposed in this study.

1.2 CO$_2$ emissions and Carbon Footprints

The proposed approach of using steel powder as an additive in producing concrete for RFHS has a triple benefit from an environmental perspective.

1. It allows for the repurposing of steel powder material.
2. It would also increase RFHS efficiency, reducing the energy demand for water heating. For example, Miriel et al. (2002) showed potential energy savings of up to 30% in a radiant heating panel.
3. Furthermore, the anticipated reduction of the peak energy demand by allowing lower temperatures for the water used in RFHS makes the use of both solar water heating and heat pumps more practical, hence supporting the phasing out of gas heating.

1.3 Radiant Heating

1 Pipes embedded in concrete has been the predominant method of RFHS since the early 20th

2 century and until the 2010s. However, radiant heating has developed significantly more

3 recently with greater emphasis on reducing climate change prompting an increase into green-

4 house gas reducing technologies which RFHS falls into. The research into RFHS is broad and

5 rapidly expanding. This includes replacing the conventional polybutylene pipes with capillary

6 tubing (Cho et al., 2019, Jobli et al., 2019) being the most groundbreaking in increasing a

7 conventional RFHS ability to heat a room quickly efficiently. Cho et al. (2019) study revealed

8 a decrease in the lag time of a capillary RFHS by 65% compared to the equivalent slab with

9 conventional tubing and increased the thermal efficiency by 9.2% at 40°C.

10

11 Sattari and Farhanieh (2006) suggest that pipe diameter and material had negligible effect on

12 heat transfer, which was contradicted by research carried out by Cho et al. (2019) and Jobli et

13 al. (2019). This difference in findings is most probably due to the differences in methodology.

14 Cho et al. (2019) maintained a consistent flow rate and volume through the PB and CT slab.

15 In contrast, Sattari and Farhanieh (2006) reduced the volume and increased the flow rate when

16 reducing the pipe diameter. Sattari and Farhanieh (2006) did show that the slab thickness and

17 cover had a large impact on the rate and quality of heat transfer with the rate and efficiency of

18 heat transfer reducing as cover increased. In a lot of structural slabs built as the foundation

19 however it is not a possibility to have a thin slab or provide minimal cover due to the slab being

20 load bearing. It is not an option to suspend a pipe at the top of a pour as there are large risks

21 and labour costs involved therefore, to make RFHS more practical, improving the thermal

22 conductivity of the concrete will improve RFHS usability by allowing deep slabs and large

23 cover. This will make RFHS a more attractive heating solution in a wider range of structures.

24

Romani et al. (2017) provided research into operating schedules for concrete considering thermal comfort, energy savings and economic savings. They concluded that the slow response of the RFHS continuous running provided the best balance for all fields. However, by increasing the thermal conductivity of the concrete, the heating system could be more adaptable, allowing for more occupancy scheduled operation allowing for lower energy use as the system is predominantly used during building operation. The purpose of this research is to increase the thermal conductivity of concrete, thereby reducing the water temperature required to achieve comfortable heating and seeing how this affects the thermal mass properties of the slab. The increasing of thermal conductivity in the slab is expected to reduce the lag time in slab warm-up, increase the slab's flexibility for changing heating cycles at shorter notice as well as providing better conductivity between the slab and heating element, reducing the heat loss and also providing a higher average temperature on the surface of the slab and therefore quicker concrete to air heat transfer.

Cho et al. (2019) researched replacing the conventional piping with smaller spacing but smaller diameter capillary pipes arranged into a capillary tube (CT) mat, which provided more significant heat transfer from the water to the concrete. The Korean standard RFHS of polybutylene (PB) pipe was compared against the CT mat. Experimental tests and simulations showed that the capillary tubes gave a more uniform temperature, higher charge rate and shorter charge time than the conventional PB pipe. The results were remarkable in that capillary tubes with 40°C water could heat the room to 20°C in 2/3 the time PB could do the same with 55°C. The research also highlighted the negative effect of lag time with radiant floor heating; when the air chamber reached 20°C the hot water supply would be stopped and subsequently restarted when the chamber cooled to 18°C. With the CT mat the floor surface temperature had a maximum variation of 1.7°C as the CT could quickly transfer heat into the slab due to the large

pipe to concrete surface area. However, the PB pipe had a maximum temperature difference of 17.6°C as the PB pipe could not transfer heat as quickly to the concrete. The slab surface of each test are shown in Figure 1, which shows 100% of the surface of the CT slab is at the highest temperature whereas, 40% of the PB slab is at the highest temperature resulting in a slower slab to air heat transfer.

Figure 1: Schematic infrared images for concrete slabs incorporated with capillary tube and polybutylene pipe (adapted after Cho et al. 2019).
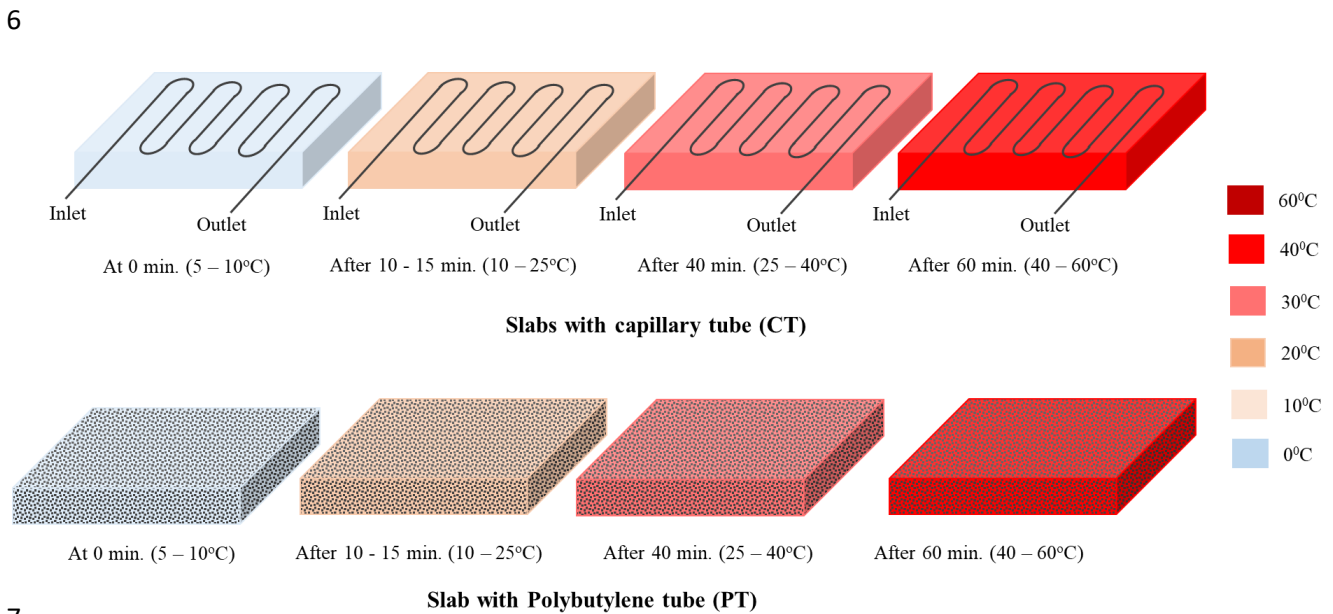
Research done by Fontana (2017) showed that the thermal conductivity of concrete with metal elements could be increased by up to about five times. This research was done using metal cylinders lying parallel to the surface of the concrete. Cook and Uher (1974) researched the thermal conductivity of steel and copper fibre-reinforced concrete, concluding that steel fibres had a lesser effect than copper fibres in increasing the thermal conductivity. Copper was much cheaper material in 1974 and has inflated 2700% to 2020. In contrast, steel has seen a slower increase in price. As a result, despite coppers' increased capability to increase thermal conductivity, steel is deemed a more viable future rollout due to lower costs and easier

accessibility to fibrous form. Cook and Uher (1974) established Equation 1 for the expected increase of thermal efficiency when adding steel fibres as an additive. This would give a high estimate of a thermal efficiency increase of 6.58% with the 12.4% replacement used in this study.

$$\frac{\lambda^*}{\lambda_0} \cong 1 + 0.45\ c_\% \text{... } Equation\ 1$$

Cook and Uher (1974)also found that vibration of the concrete during manufacture produced an alignment of fibres which meant that theoretical methods based on a random fibre distribution under-estimated the experimental values. As powder in this study is being used, it is expected that vibration will have no effect on aligning particles and will not affect the thermal conductivity. Steel fibres have been used in other studies to improve the thermal conductivity in concrete. Most research shows that an increase in steel content always leads to increased thermal conductivity (Cook and Uher, 1974, Tinker and Cabrera, 1992). However, the relationship between conductivity and thermal mass is yet to be investigated. Saminda et al. (2019) researched the mechanical improvements given by implementing steel fibres. According to Saminda et al. (2019), a selected replacement of 0-1% showed an increase in 17-20% compressive strength using fibres with an average length of 37mm and diameter of 0.42mm. This phenomenon was similar to that used by Cook and Uher (1974) however these large fibers when used can cause huge issues with pumping, which is often the only option for large floor areas and areas with poor accessibility. They also severely limit the volume of steel fibres that can be used, thereby limiting the maximum thermal conductivity of the concrete.

The studies carried out by both Cook and Uher (1974) and Saminda et al. (2019) used steel fibres for either mechanical improvements or thermal conductivity improvements respectively. However, this approach can often cause expensive problems and mistakes when the concrete

is pumped (the pumps can become blocked), leading to a worst-case scenario of having to stop mid pour and blocking the pump and lines. This has led to several significant court cases in the US and likely lower profile cases in the UK. On the other hand, the use of fine maraging steel, which is a powder and granular-like rather than fibrous, makes the mix more similar to a standard mix and therefore unlikely to cause issues when pouring. Hence, it allows a much higher replacement content without reducing workability and, ideally, strength.

The compressive strength of the mix will be investigated in this study since this has not been tested before either using powdered steel or for such a high proportion of steel in the concrete mix. Where steel fibres are used in concrete, it can increase tensile strength. However, fine steel powder will not provide this benefit. On the other hand, using steel powder instead of sand means that the concrete absorbs less water, resulting in a stronger mix whilst remaining workable. This will theoretically increase the compressive strength which for RFHS is an important value. This highlights the importance of compressive testing to confirm the slab's capabilities in compression. Theoretically, the compressive strength could vary significantly and could even rule out this approach.

Therefore, this paper investigates an approach for increasing the thermal conductivity of concrete to reduce the temperature differential across the slab by using some material additives. It is expected that a more uniform high temperature across the slab would allow for a greater rate of heat transfer from the slab to the surroundings and also enhance sustainability.

2.0 Materials

The materials used for this research were Portland cement - PC, sand, grit, steel powder, coarse aggregates, thermocouple, heating pipe and plywood. PC was manufactured in compliance with BS EN 197-1:2011 and supplied by Lafarge Cement UK. The thermocouple used is the

K-type with a temperature range of -200 to 1260°C (-326 to 2300°F), and was supplied by TC Ltd, UK. A low carbon steel (Maraging steel) was used as fine aggregate in the form of a very fine powder (circa 40 μm) with a thermal conductivity of 14.2 W/mK at 20°C (Renishaw, 2017). The plywood was obtained from a local manufacturer in Bristol, UK. Coarse aggregate of sizes 4/10 and 10/20, and natural sea-dredged sand from the Bristol Channel supplied by a local quarry and complied with the requirements of BS EN 12620:2002+A1:2008 were also used throughout the study.

3.0   Methodology

The project assessed the capabilities of increasing the thermal capacity and conductivity of concrete slabs to reduce the temperature differential across the slab. A uniformed high temperature across a concrete slab reminiscent was designed and constructed to allow greater rates of heat transfer from the slab to the building surroundings as shown in Figure 2. Two concrete slabs of dimensions 400 (width) × 400 (length) × 200mm (depth) were constructed from the formwork in Figure 2 with straight sections of the heating pipes running through at centre height. Figure 3 shows a cross-section of the slabs. It is important to note that the depth of the concrete slab in the model was built to increase the accuracy and reliability of the results, while Figure 3 shows a cross-section of the slab.

Figure 2: Test slab formwork before concrete pour
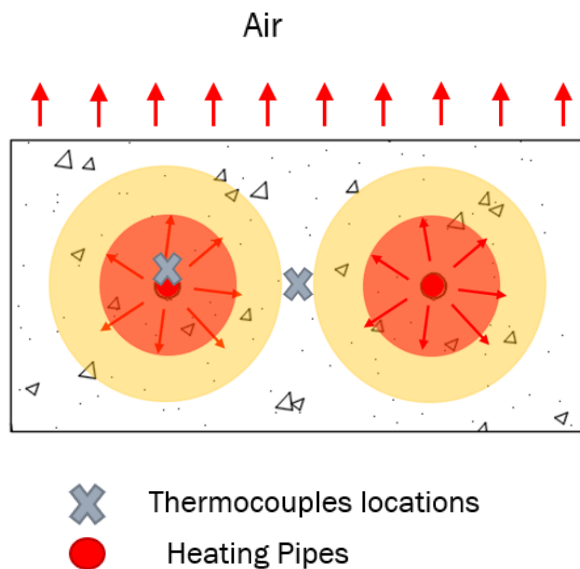
Figure 3: Cross section of test slab

The heating pipes contained an inner and outer layer of Polyethylene of Raised Temperature (PE-RT) tubing with an aluminium intermediate layer allowing the pipes to remain rigid during the concrete pour and vibration, whilst still being sufficiently flexible and inelastic, to allow shaping bends into the pipes. The pipes were laid to manufacturer's instruction with a maximum bending radius of 100 mm. The bend was outside the concrete slab to provide secure fixing for the pipes and a uniform section of pipe spacing for testing (see Figure 2). The

thermocouples were fixed using steel reinforcement tying wires and tying tools, to hold the

thermocouples securely during the concrete pour.

3.1 Concrete Mix Design

The base mix was C35 mix (concrete strength of 35 Newtons after 28 days) used for the Normal

Mix (NM) slab and adapted for the Steel Mix (SM), shown in Table 1. The 35 N, 28-Day

strength concrete is mainly used for external slabs regarding heavy duty applications, where

the ground conditions are subjected to frequent heaving loading from foot traffic and heavy

vehicles. This is suitable for indoor floor slabs containing metal and is resistance to a freeze-

thaw cycles due to additives (Levy, 2012; iMix Concrete 2022). 70% of the sand in the SM

was swapped by mass for the steel powder, resulting in a net 12.4% of steel by volume. From

equation 1, this is expected to produce an increase of 6.58% in thermal efficiency. A C35 mix

has a higher cement content inclusion, meaning that the strength of this mix is in the higher

class of the design concrete slabs, when strength is a factor for the concrete application.

Nevertheless, a high water/cement ratio without the appropriate concrete setting time can lead

to a high and rapid expansion of the slab and further cracking within RFHS slabs at early and

late hydration stages.

Table 1: Concrete mix for NM and SM slab

C35 Mix	Cement	Water	Fines			Coarse		Total
			Sand	Grit	Steel	4/10	10/20	-
1m² ratio	395	200	231	429	0	585	585	-
Conventional	13.430	6.800	14.586	7.854	0	19.890	19.890	82.45

Steel Slab	13.430	6.800	4.376	7.854	10.210	19.890	19.890	82.45

3.2 Concrete Slab Crushing tests

The mix compressive strength was tested using 3 $0.1 \times 0.1 \times 0.1$m cubes for a normal (NM) C35 mix design and steel (SM) mix design which are to be tested 28 days after forming and the weight and crushing strength recorded. The C35 NM slabs/cubes are being tested to verify the method as these cubes should be stronger than or very close to 35MPa crushing strength, if they are not, the mix will have to be tested again. The cubes will be weighed and then crushed using an Avery Denison Cube Crusher shown in Figure 4 28 days after casting. Once the experimental slabs/cubes were crushed, they were viewed under an electronic microscope to see how the steel reacted with the concrete.

The density of concrete mixed with steel fine powder will increase and the compressive capacity decrease at elevated temperatures (100 °C to 200°C). Research by Zheng et al. 2013 on the compressive and tensile properties of reactive powder concrete (RPC) with steel fibres at elevated temperatures found that at temperatures below 300 °C cubes' compressive strength of RPC increases as the steel fibre content increases but decreases between 400 and 800 °C as steel fibre content increases. As temperatures in the testbeds did not exceed 60°C and on the compressive and tensile experimentation performed, the structural integrity of the slabs for both SM and NM were not compromised. Distinct changes in the microstructure of concrete with steel fibre content changes in the microstructure and the mechanical properties alters from a macro perspective. Data generated from experimental test can be utilised in developing relations for expressing the mechanical properties as a function of temperature and address the influence of the structural integrity of the slabs.

Figure 4: Avery Denison cube crusher

The cover, cross-section and depth of the tow slabs were identical from the results to be transferable and the cover to the pipes can be a major affecting factor (Sattari, *et al.*, (2006). Maraging steel was used, a low carbon steel, a very fine powder circa 40 μm with a thermal conductivity of 14.2 W/mK at 20°C (Renishaw PLC, 2017), hence the thermal conductivity, k value for steel was selected as 14.2 W/mK and for concrete 0.7 W/mK. Temperature probes and sensors were placed in 3 locations across each slab using K-type thermocouples (TC Ltd. Model number: A50) within the slab as shown in Figure 2 and 3. The inlet water and room temperature were recorded using identical thermocouple probes throughout the tests. Recording starts consecutively with the heating and pumping of the water from ambient room temperature (22 to 25°C). The heating was predominantly tested between 8 AM to 4 AM and then cooling was recorded overnight in a temperature-controlled room. Water temperatures ranging from 40-60°C were used for the experiments. The lower temperature range and boundary conditions were chosen to replicate similar energy systems such as heat sources from solar water heaters or thermal energy extracted from ground-source heat pumps. These systems are becoming quite relevant across the UK within the built environment. Water temperatures above 60°C provided the upper boundary conditions within the concrete slabs.

3.3 Thermal Response Experiments

The concrete slabs with the heating pipes were subjected to 3 different types of testing for the temperature range of 40-60 °C. The slabs were left for 24 hours to acclimatise to the room temperature and environmental conditions before testing. There was a minimum of 12 hours between each test to allow the slabs to achieve uniform ambient temperatures. It was also found from the initial thermocouple readings that the hydration rates slowed to a level that would not impact the temperature recordings during the heat distribution tests (Miriel, J et al 2002 ; Cho, J et al (2019). All tests were recorded using a pico logger and the picolog 6 software. Readings were taken at 10-minute intervals when the heater and pump were turned on. The infrared images were taken using the FLIR TG275 camera with an accuracy of +/- 3°C in the temperature range of the test.

3.4 Experimental Testing

The project tested the reliability and accuracy of the experimental setup and the comparison of heat transfer rates across the various slabs and analysed their thermal properties (heat storage and transfer). The concrete slabs were connected to a peristaltic water pump (Welco Japan) and the heating pipes/tubes. The water started off at ambient temperature and was pumped through the slabs at a flow rate of 2.0 L/min. The heating coil/tubes were set to raise the water temperature to the target value. The SM and NM slab were heated for the same amount of time. It was found that 3.3 hours was the ideal heating period, and the slabs were then left to cool prior to analysis. After the heating period was switched off, the thermocouples continued to record for a minimum of 4 hours to gather information on the slabs' ability to store heat. For the second testing phase, the slabs were allowed to reach peak temperatures, and infrared

1   images were taken of the surfaces to show the heat distribution. The average heat distribution

2   across the surface corresponds with the slabs ability to transfer to the air surrounding its surface.

3   Thermocouple readings of the slab at a steady temperature state would also be used to get a

4   value for the rate of heat transfer of each concrete mix at 40°C and 60°C by using Equation 6

5   of the multi-layered cylinder theorem. The water temperature was set to the test temperature

6   and flow rate set to 4.0L/min. The slabs were then left until the surface temperature was

7   constant at +/- 0.5°C for 30 minutes. Infrared images were taken at the surface, and readings of

8   the thermocouples throughout the slab. The third phase of testing modelled the heating of the

9   enclosed spaces by placing a 400 Test 3 models the heating of an enclosed space by placing a

10 400 × 400 × 400 plywood box over the top of the slab. This test generated the values required

11 for Equations 2 and 3 for heat transfer efficiency across each slab.

12

13

14

15 3.4.1   Thermal and Energy Efficiency

16 The thermal and energy efficiency was computed using equations 2, 3 and datasets from tests

17 3. The energy input and energy output of the slabs was calculated, allowing for the energy

18 efficiency of each slab to be compared. Each slab was heated for approximately 10 hours until

19 the slab surface was at a constant temperature +/- 0.5°C for a minimum of 30 minutes to record

20 a value for ΔT_{ra} for the temperature about the slab. This provides a numerical value for each

21 slab's input energy, output energy, and efficiency at the heating range of 40° - 60°C

22 respectively. The Temperature Differential for hot water (ΔT_{hw}) was taken as the test

23 temperature minus the recorded water temperature recorded as the recorded temperature shows

24 the return water temperature. The values for Cp_{hw} (4.19kJ/kg °C), Cp_{air} (1.00 kJ/kg °C), ρ_{hw}

1   (997kg/m³) and ρ_{air} (1.225kg/m³) were used in accordance with Baehr and Stephan (2011)

2   and V_{tr} was 0.064m³ contained in a 400mm wooden cube mounted on top of the slab with the

3   surface mounted thermocouple recording the temperature change in the cube from the start of

4   the test to the constant slab surface temperature reading.

5

6                $q_{hw}^{in} = Q_{hw} \times \Delta T_{hw} \times Cp_{hw} \times \rho_{hw}$ Equation 2

7

8                $q_{ra}^{out} = V_{tr} \times \Delta T_{ra} \times Cp_{air} \times \rho_{air}$ Equation 3

9

3.4.2   Multi-layered Cylinders

11   The rate of heat transfer of each slab was computed using equation 6 (derived from equations

12   4 and 5) using the data from the tests as illustrated in Figure 5. The temperatures were taken

13   adjacent to the pipes and at the slab surface, T_1 and T_3 respectively. The concrete and steel

14   would be assumed as separate layers, and the outermost layer will have a tangent along the slab

15   surface. The calculations used steel as the internal layer and once again as the external layer.

16   The results were averaged to give a result for each slab's heat transfer rate. The values for the

17   radius, r of each layer is calculated using the known r_3 value of 100mm and the proportions of

18   the mix from Table 1 to give values for r_1 and r_3.

19     $(T_1 - T_3) = (T_1 - T_2) + (T_2 - T_3)$ Equation 4

20

21     $Q = \dfrac{2\pi\, k_a\, (T_1 - T_2) \times L}{\ln\left(\frac{r_2}{r_1}\right)} = \dfrac{2\pi\, k_b\, (T_2 - T_3) \times L}{\ln\left(\frac{r_3}{r_2}\right)}$ Equation 5

$$Q = \frac{(T_1 - T_3)}{\frac{1}{2\pi \times L \times k_a} \times \ln\left(\frac{r_2}{r_1}\right) + \frac{1}{2\pi \times L \times k_b} \times \ln\left(\frac{r_3}{r_2}\right)} \qquad \text{Equation 6}$$
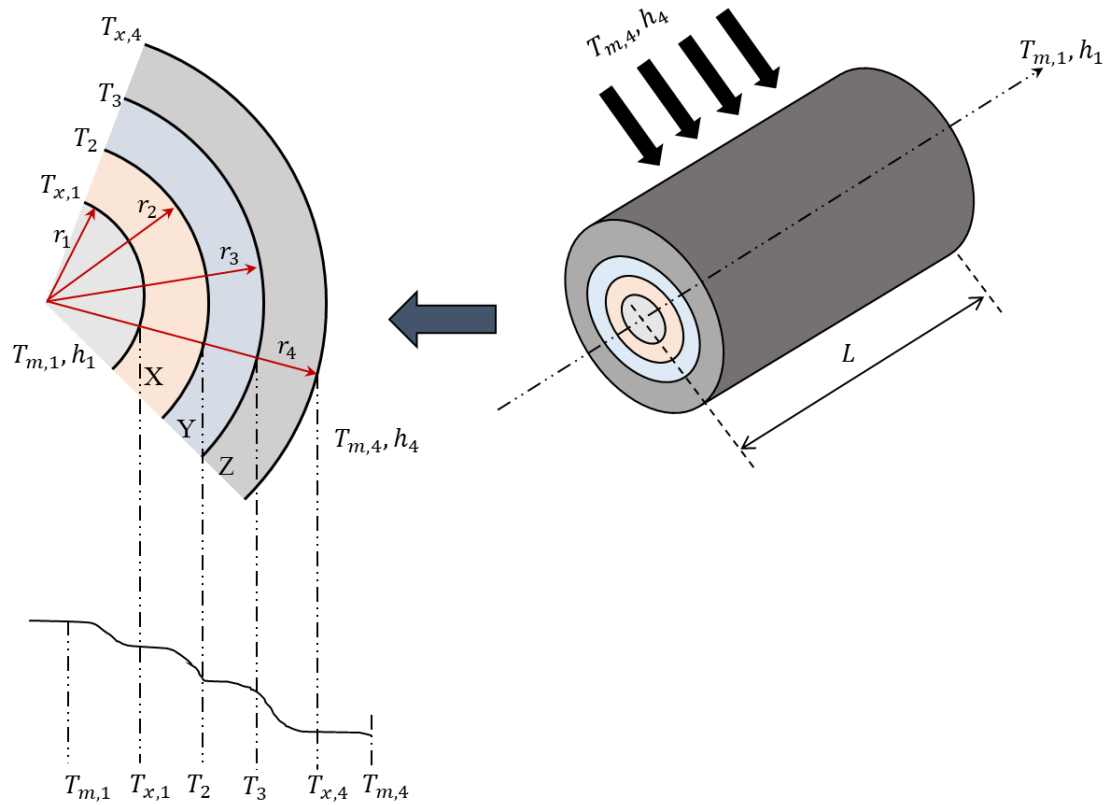
Figure 5: Tubes with three layers of varying thermal conductivities (adapted after Das, 2010)

4.0   Result analysis

4.1   Unconfined compression strength (UCS) test

Table 2 shows the UCS test and measured density results for the concrete cubes after 28 days of curing in water. Observation showed an average increase in density of 4.5% in the concrete produced from the steel mix compositions compared to the control mix (composition with sand). This phenomenon is expected due to the considerable higher density of steel than the fine sand. However, the UCS was reduced to 74.0% of the normal mix, a significant drop in the strength behaving closer to a C25 mix.

In addition, the concrete cube made from the steel mix composition displayed a variation in weight of 1.3% compared to 1.4% for the control mix. The steel mix and control mix cubes showed similar variations in weight of 1.3% and 1.4% respectively. The steel mix showed a higher variation in the stress of 5.9% compared to 2.8% for the NM. However, this is partly attributed to the average stress of the SM being considerably less than the NM.

Table 2: Cube crushing test results Table 2 (in accordance to BS EN 197-1,2011 specifications) :

Cube	Weight, g	Stress, MPa
Steel Mix		
1	2449.6	24.62
2	2430.5	25.45
3	2417.0	23.99
Average	**2432.4**	**24.69**
Normal Mix (Control)		
1	2306.6	33.13
2	2339.9	32.99
3	2332.8	33.93
Average	**2326.4**	**33.35**

4.2   Thermal analysis

Figure 6 shows the results of the temperature transfer for the control mix (Normal Mix) with the water cut-off at 05:50:00. It was observed that the water takes 31 minutes to reach a temperature of 57°C, while the adjacent to pipe temperature increases rapidly at 3.1min/°C during the heating period and achieved a temperature of 36.18°C in the same period with the temperature rate reducing to 39.11min/°C after 00:37:00 uniformly until shut off at 05:50:00. Furthermore, the temperature adjacent to pipe decreases exponentially from shut off. The slab centre temperature has a lag time of 26 minutes to have a significant reaction to the heating and from this point heats at a uniform increase rate of 24.4 min/°C until at 06:03:00, 13 minutes after the heat and pump shut off. From 07:17:00 the slab centre and adjacent pipe decrease exponentially at the same rate until the end of the test. The water temperature peaks at the start of the test at 57°C but decreases to 54.9±0.82°C as the water transfers heat into the slab as it is pumped. For the same reason, the water temperature has a high point at the end of the test when the pumping is stopped but heating element is still hot.
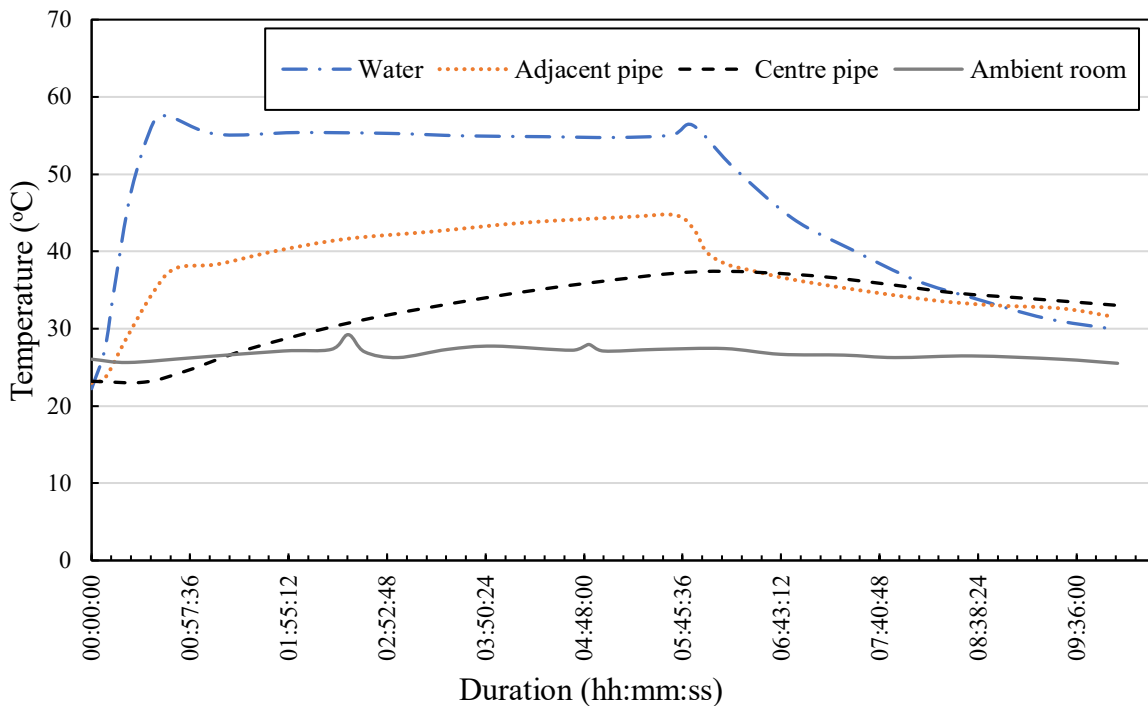
Figure 6: Temperature measurement for Normal Mix (NM) slab 1 with heater cut off at 05:50:00

21

Figure 7 shows the results for shows the results of the temperature transfer for the control mix with the water cut-off at 03:15:00. Observation showed that the temperature of 59.57°C is reached after 36 minutes, while the adjacent to pipe temperature increases rapidly at 2.65min./°C during this heating period, reaching 37.68°C in the same period with the temperature reducing to 28.32min/°C after 00:38:00 until water cut-off at 03:15:00. However, the temperature adjacent to the pipe decreases exponentially from the cut-off.

It is also important to note that the slab centre temperature has a lag time of 29 minutes to impact a significant reaction to the heating, hereby, produces an increase in heat at a uniform rate of 18.93 min/°C until 03:48:00, 32 minutes after the heat and pump is cut-off. From 04:48:00 up awards, the slab centre and adjacent pipe decreases exponentially at similar rates until the end of the test. Hence, the water temperature peaks at the start of the test at 59.57°C but decreases to 57.01±0.22°C as the water transfers heat into the slab when pumped in an ambient room temperature of 22.50°C±1.27°C.
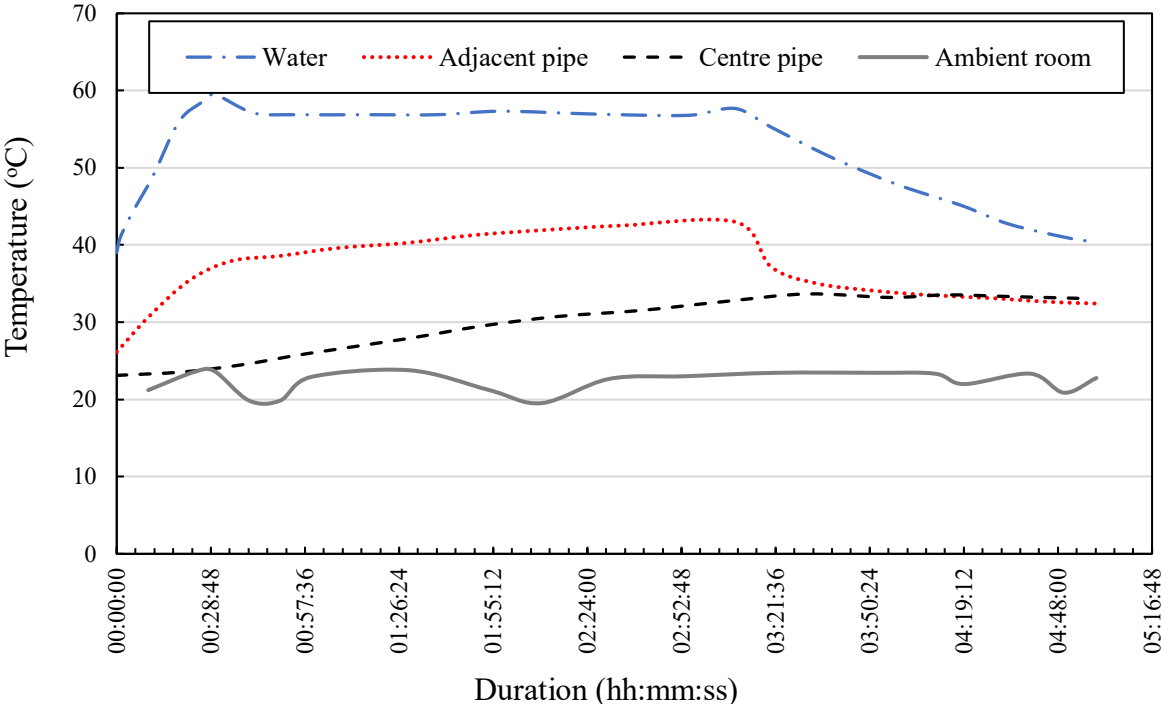
Figure 7: Temperature measurement for Normal Mix (NM) slab 1 with Heater cut-off at 03:15:00

Figure 8 shows the results for shows the results of the temperature transfer for the steel mix slab 1 with the water cut-off at 03:30:00. It was observed that the water temperature takes 34 minutes to reach achieve 60.16°C. The adjacent to pipe temperature increases rapidly from 2.50min/°C to 39.48°C in the same period. However, the temperature uniformly reduced to 32.15min/°C after 00:38:00 until cut-off at 03:30:00. However, the temperature adjacent to pipe decreases exponentially from shut off.

Furthermore, the slab centre temperature has a lag time of 22 minutes to produce a significant reaction to the heating and from this point heats at a uniform increase rate of 19.6 min/°C until at 03:55:00, 25 minutes after the heat and pump shut off. It is worth noting that from 05:00:00, the slab centre and adjacent pipe decreases exponentially at similar rates until the end of the test. The slab surface starts at 24.67°C and starts to increase at 01:10:00, reaching a peak of 30.36°C at 04:20:00, 50 minutes after the cut-off. The water temperature peaks at the start of the test at 60.2°C but decreases to 57.09+/- 0.17°C as the water transfers heat into the slab as it is pumped in an ambient room temperature of 23.38 °C±0.93°C.
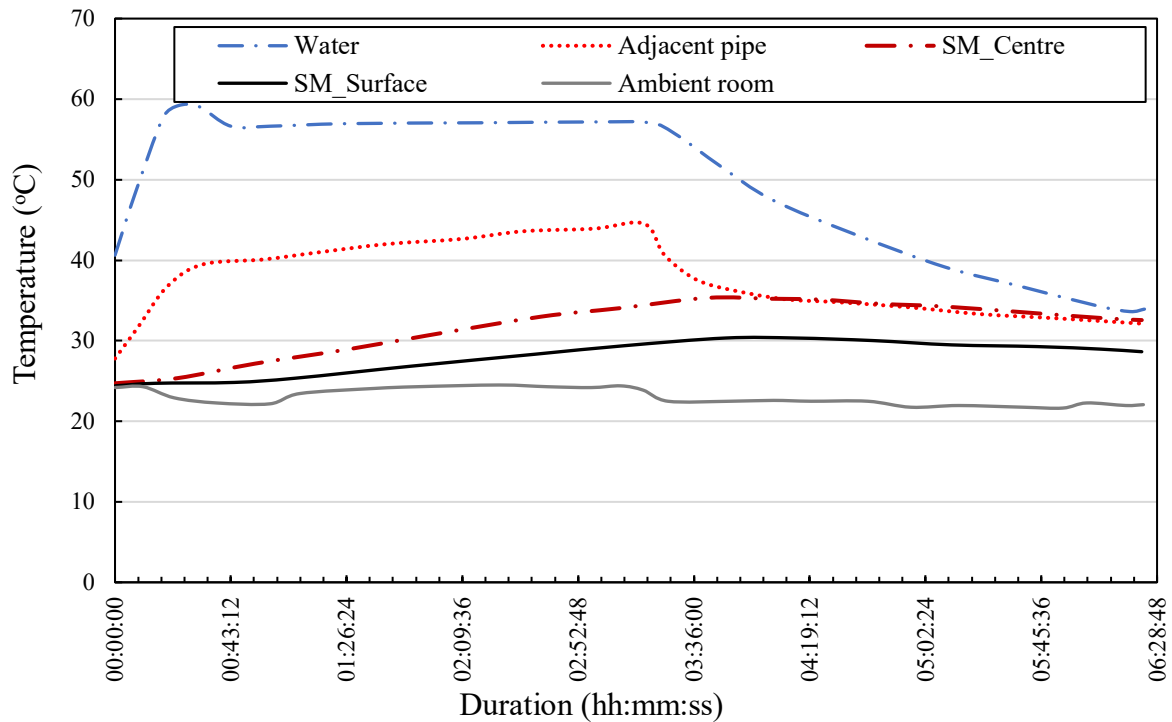
Figure 8: Temperature measurement for Steel Mix (SM) Slab 1 with Heater cut-off at 03:30:00

Figure 9 shows the temperature transfer for the Normal mix slab 2, which the water was cut-off at 03:30:00. It was observed that it takes about 32 minutes for the water to achieve a temperature of 59.3°C at a rate of 0.90 min/ °C. In contrast, the adjacent pipe temperature rapidly increases at 2.44min/°C during this heating period to achieve a temperature of 37.88°C in the same period. However, the rate of temperature increase reduces uniformly to 27.60min/°C after 00:36:00 until water cut-off at 03:30:00, while the temperature adjacent to pipe decreases exponentially from shut off. The temperature at the centre of the slab has a lag time of 23 minutes to enable a significant reaction to the heating and from this point heats at a uniform increase rate of 19.0 min/°C until at 04:03:00, which is 27 minutes after the heat and pump are shut off.

Observation also showed that from 05:11:00 the slab centre and adjacent pipe decreases exponentially at similar rates until the end of the test. The slab surface temperature commences at 23.83°C and increases at 0:36:00 reaching a temperature peak of 31.55°C at 04:16:00, which

is 46 minutes after the shut-off. Finally, it is worth reporting that the water temperature peaks at the start of the test at 59.3°C but decreases to 56.54± 0.14°C as the water transfers heat into the slab while being pumped at an ambient room temperature of 24.27°C± 0.28°C.
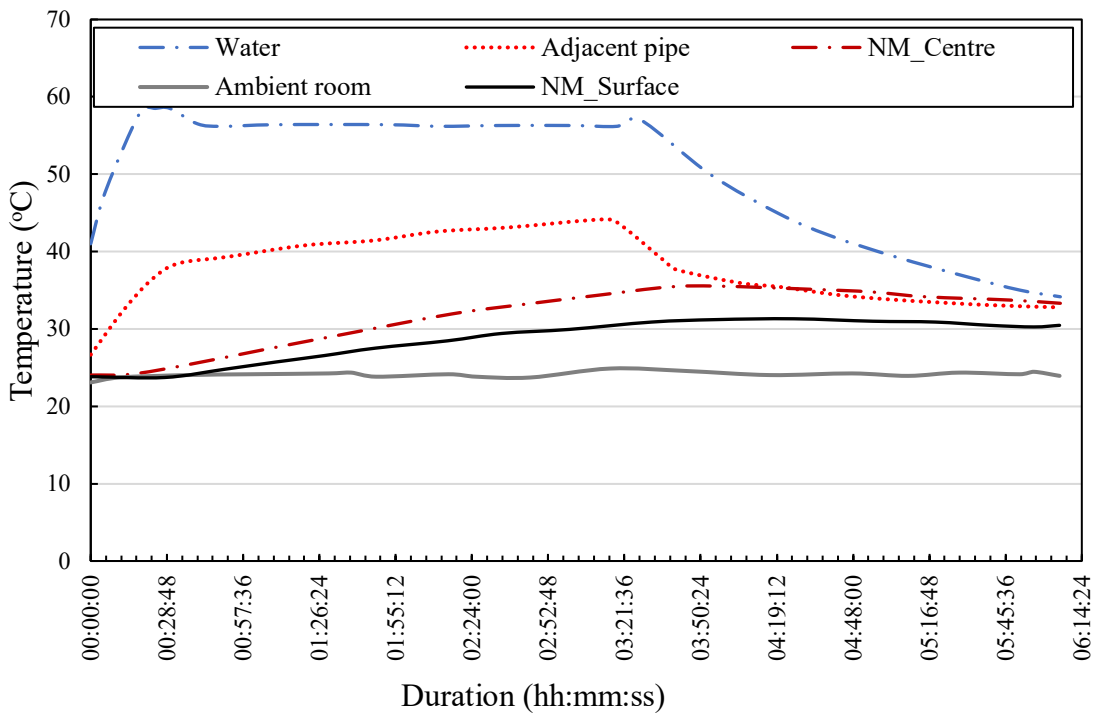
Figure 9: Temperature measurement for Normal Mix (NM) slab 2 with Heater cut-off at 03:30:00

Observation showed that the Normal mix slab 3 test in Figure 10 was cut off at 07:34:00. The water attained a temperature of 39.82°C after 20 minutes at a rate of 1.32 min/°C, while the adjacent to pipe temperature increases rapidly at 5.49min/°C during this heating period to attain a temperature of 31.12°C. Furthermore, the rate of temperature increases uniformly reduced to 116.76min/°C after 00:24:00 until shut off at 07:34:00. However, the temperature adjacent to pipe decreases exponentially from shut off. The slab centre temperature has a lag time of 22 minutes to enable a significant reaction to the heating and from this point heats at a average increase rate of 70.19 min/°C until at 07:54:00, which was 20 minutes after the heat and pump shut off.

1   It was also established that after 08:31:00, the temperature of the centre of slab and adjacent

2   pipe decreases exponentially at similar rates until the end of the test. The slab surface starts at

3   25.06°C and decreases to 24.67°C at 00:30:00, and then increases to 29.33°C at 08:05:00 which

4   is 31 minutes after the shut-off. Additionally, the water temperature peaks at the start of the

5   test at 39.83°C but decreases to 38.41± 0.11°C as the water transfers heat into the slab as it is

6   pumped at an ambient room temperature of 25.22°C±0.48°C.
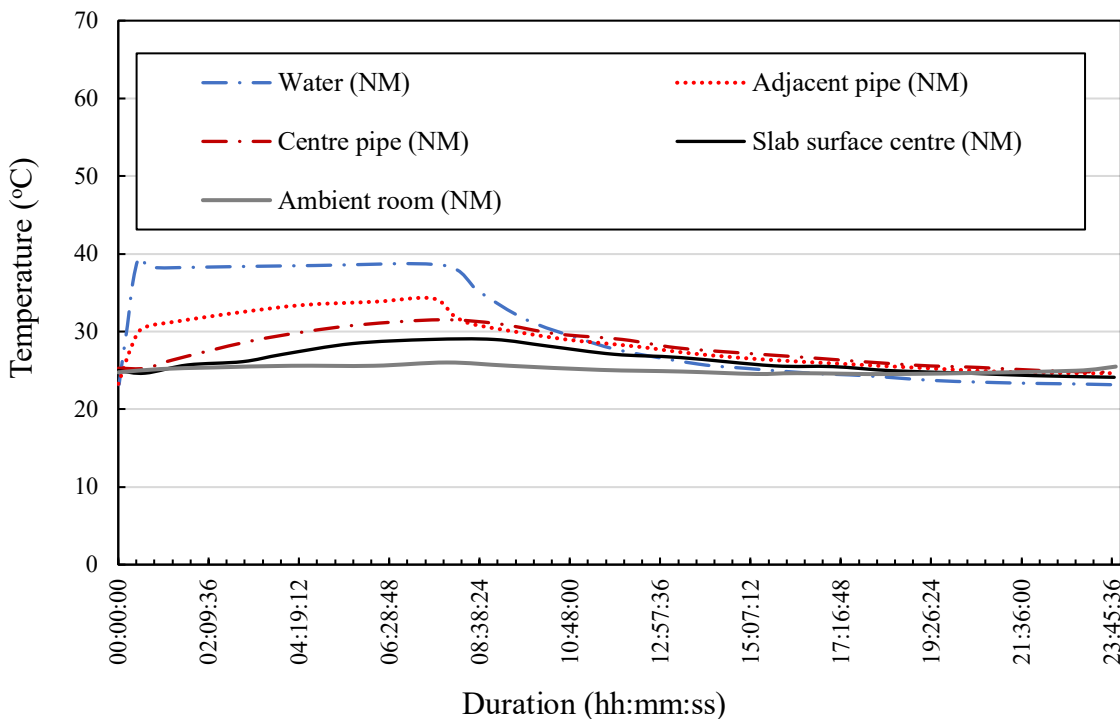
7
8   **Figure 10:** Temperature measurement for Normal Mix (NM) slab 3 with Heater cut-off at 07:34:00
9

10   Figure 11 shows the results for the temperature transfer for Steel mix slab 2 at 07:05:00.

11   Observation showed fluctuations in the water temperature due to low water levels in the tank,

12   meaning parts of the heating elements were not covered. Afterwards, the tank was refilled at

13   03:30:00, but the water temperature remained high for the rest of the test. As a result,

14   comparing the tests at 40°C would be unreliable.
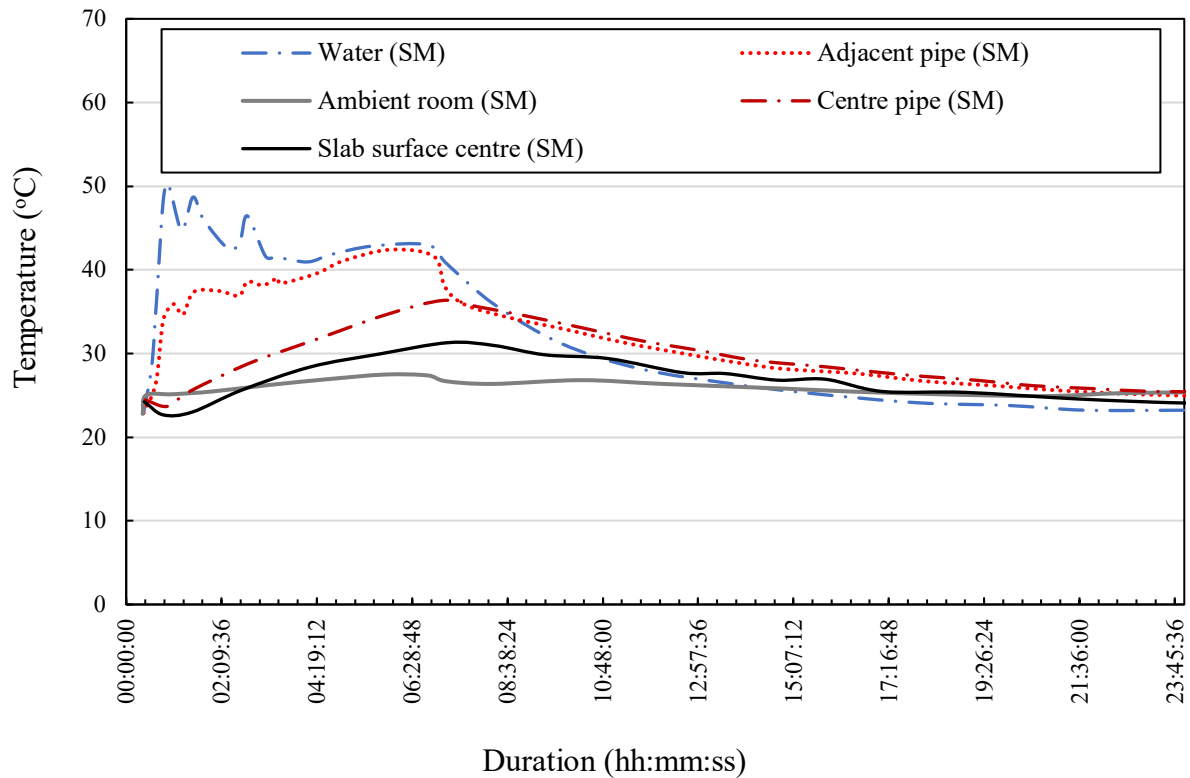
Figure 11: Temperature measurement for Steel Mix (SM) slab 2 with Heater cut-off at 07:05:00

5.0 Discussion

5.1 Compressive Strength analysis

The potential for strength gain of the developed SM is a direct potential of its application as a construction material. However, the observed 26% reduction in the investigated SM concrete specimens' average stress could be dues to the lower bonding capacity of the produced hydration cementitious hydrates with the steel powder granules, resulting in weak joints that cannot withstand the applied load. Another factor could also be due to the smoother edges of the steel powder than sand, which has a small amount of internal friction compared to sharp sand, resulting in the steel powder having a lower compressive strength. Furthermore, the steel replacement is made up of finer particles than the sand, as a result, it disturbed the balance of aggregates in the concrete mix. Also, the steel cannot absorb water such as sand; therefore,

27

there were residual water pockets within the slab, increasing the porosity and causing weak points.

The standard mix slabs for comparison also had poorer than expected results in the strength tests. It was a C35 mix so only 5% of cubes should have had a value below 35MPa, whereas the cubes that were tested all had values below 35MPa. This raises the question of whether there was an additional factor that contributed to the poor results in both mixes, such as human error or partly hydrated cement used in the mixing. In this case the crushing strength may have not been reduced to the extent shown in these results.

5.2   Thermal flux and temperature analysis at 60°C

Tests on Steel Mix slab 1 and Normal mix slab 2 are directly comparable (see Figure 12) as they are heated at the same temperature for the same amount of time. In Figure 11, the NM test is 20 minutes off set from the SM slab for ease of reading the graph. The results show that for Steel Mix slab 1, the adjacent pipe temperature increases at an initial rate of 2.50min/ °C, subsequently dropping to a rate of 32.15min/ °C once the water had reached the target temperature of 60 °C. Normal mix slab 2 comparatively had an initial heating rate of 2.44min/ °C slowing to 27.60min/ °C once the slab had reached temperature. Although these values should be very similar as the thermocouples are adjacent to the pipes, this suggests that the thermocouple may have moved slightly during the pour, thus allowing differing amounts of concrete between the thermocouple and the pipe for the different slabs.
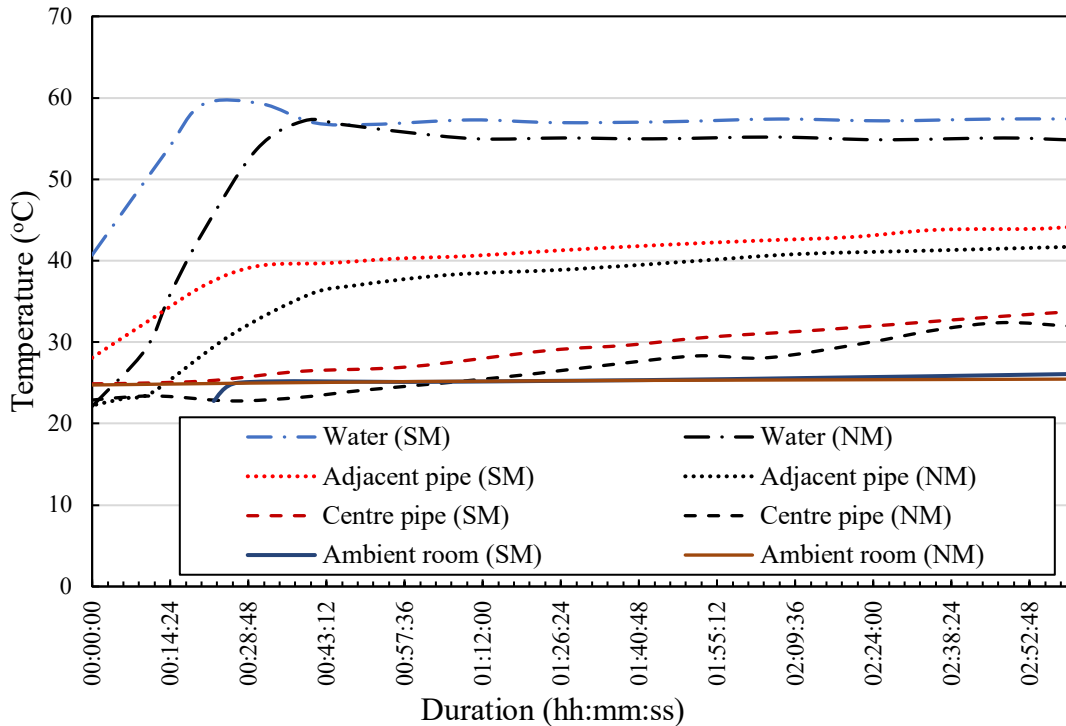
Figure 12: Normal Mix (NM) and Steel Mix (SM) test temperature comparison at 60°C showing a 20 minute off-set of the NM from the SM.

The SM and NM slabs react to the centre thermocouple at similar times of 22 and 23 minutes, respectively suggesting a slight increase of conductivity in the SM slab. This opposes the rate the slab centres heat. The SM increases at 19.6min/ °C compared to 19.0 min/ °C for NM showing the SM heat transfer rate is 97% that of the NM slab. This is shown in figure 12, if the lines showing the temperature of the slab centres was continued, the NM slab would overtake the SM slab around 05:00:00.

The slab surface measurements suggest that the SM may have reduced thermal efficiency compared to the NM slab, as under the same 3 hr 30min heating, the NM slab surface increased by 7.72 °C compared to 5.69 °C for the SM slab, a 26% reduction. The ambient room temperature was 0.89°C warmer for the NM slab, impacting the slab surface readings. The slab

centre readings also show the same trend, and these results are unimpacted by short term fluctuations in ambient room temperature. The water temperature was 0.55°C warmer during the SM tests, and despite this, the NM slab appeared to transfer heat at a higher rate.

This suggests that the thermal efficiency and rate of heat transfer may have been reduced by incorporating steel powder into the mix. An interesting observation, however, is that even though the same heating input was put into the water being pumped into each slab, there is a large difference in the rate of increase of water temperature in Figure 12. The water temperature increases more slowly in the SM slab, and this is probably caused by the slab being able to draw heat away from the pipe more quickly by spreading the heat more evenly and more widely across the slab.

During the discharge phase, once the heating element and pump had been turned off, the slab surface of both the SM and NM slab surfaces lose heat at a rate of $103\text{min}/^{\circ}\text{C}$ and $118\text{min}/^{\circ}\text{C}$ respectively. This quicker discharge rate would have been expected of the SM slab if the thermal conductivity had been increased. Therefore, the SM slab has a higher discharge rate as the heat is transferred to the surface of the slab quicker than the NM equivalent.
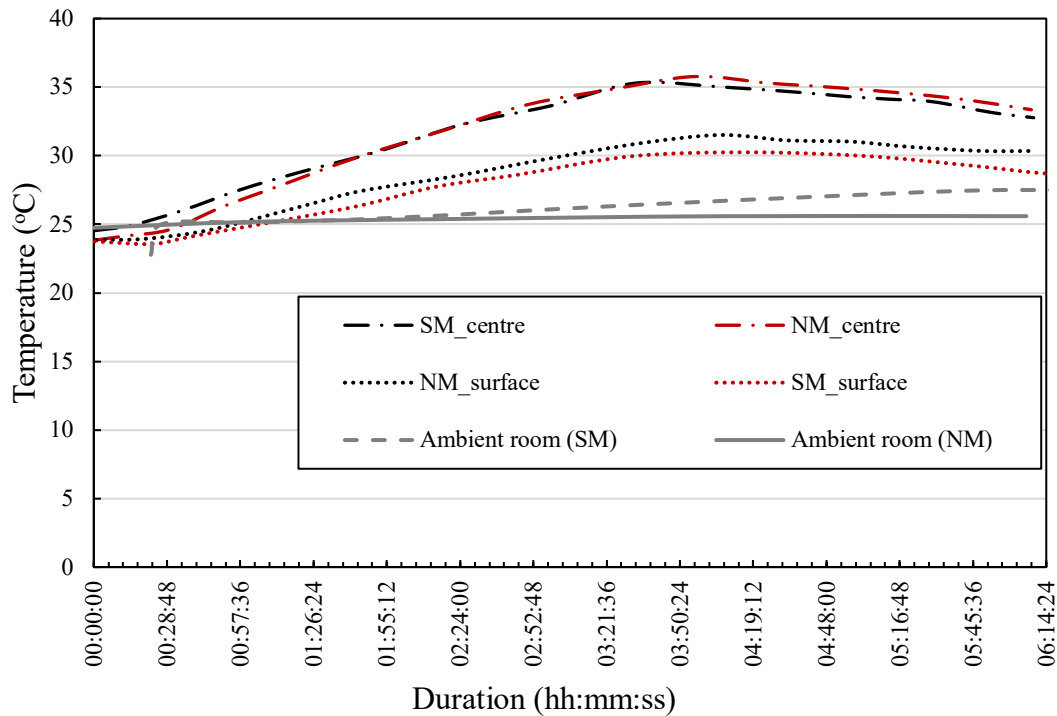
Figure 13: Slab surface and centre temperature comparison [Normal Mix (NM) and Steel Mix (SM)] at 60°C

5.3   Surfacing imaging

The infra-red imaging could only be taken during the heating of the slabs before the university was closed. Therefore, the images were taken at different intervals during the test, so the temperature values are not directly comparable. These experimental investigations were focused on analysing the characteristics of the floor temperature gradient. Radiation is the main heat transfer mechanisms occurring for the floor slabs and the radiative heat flux accounts for approximately 50-60 % of the total heat flux. However, the SM slab (see Figure 14) clearly shows a more even distribution of surface temperature, shown as orange and light green, than the NM slab (Figure 15), which shows a more severe red to orange colouring.
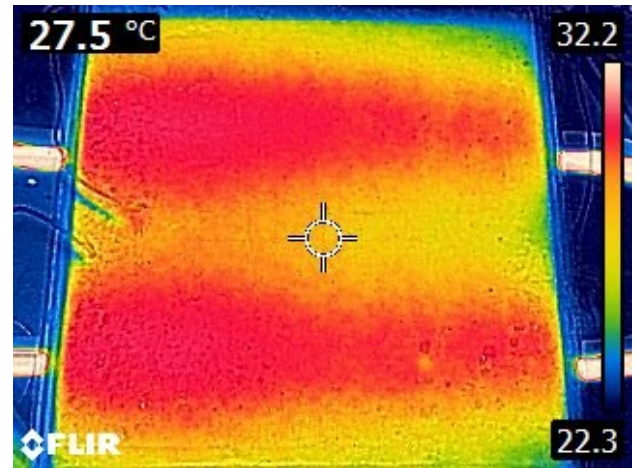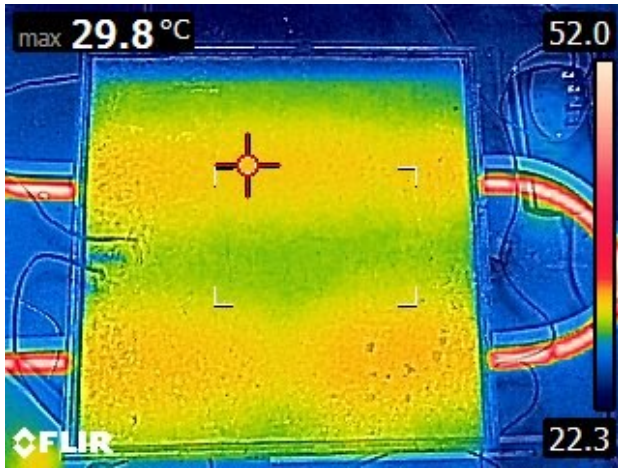
Figure 14: Infra-red image of Steel Mix (SM) slab surface   **Figure 15:** Infra-red image of Normal Mix (NM) slab

The results of the infra-red imaging for the SM slabs versus the NM slab displays (Figures 14 and 15) a variation in the consistency of heat transfer performance under the conditions of low water supply temperatures and traditional RFHS. The temperature heating profile for both slabs remains stable over time, but the temperature difference between NM slab and SM slabs and the ambient air temperature inside the controlled room fluctuates due to a variation in heat transfer, thermal fluxes and heat losses between both slabs.

5.4   Heat transfer coefficients

When computing heat transfer coefficients, it is very important in applying the appropriate reference temperatures. The total heat transfer coefficient (h_{total}) and the total heat flux density emitted from the radiant surface (q_{total})is often used in engineering practice. The heat transfer coefficient (h_{total}) is sometimes assumed as a constant around 8.5 W/m^{2}K to 11.0 W/m^{2}K (Karadağ, 2009; Fontan, 2011; Olesen and Zöllner, 2007; Hajabdollahi et al. 2012; Zhang et al.2012; Cholewa et al. 2013) .Alternative methods of computing h_{total} is the use of equation (7)

1     $h_{total} = \dfrac{q_{total}}{T_{op} - T_s}$ Equation 7

2

3   Where T_{op} is the ambient room temperature (°C) and T_s is the mean radiant surface temperature

4   of the slab (°C). For the calculations of the total heat transfer coefficient between the slab

5   surfaces and the room, two (2) operative temperatures were used at a height of 1.10 meters for

6   a standing person in the room and a height of 0.60 metres for a sitting person. The reference

7   temperatures were then calculated in a room where the air velocity can be assumed to be less

8   than 0.2 m/s and the differences between the average radiant temperature and air temperature

9   (ambient room temperature) is minimal, the following equation can be used:

10     $T_{op} = \dfrac{T_a + T_{mr}}{2}$ Equation 8

11   Where T_a is the air temperature and T_{mr} is the mean radiant temperature (°C). The value of the

12   total heat flux density emitted from both slabs (NM and SM) was computed using these heat

13   flux density equations. The total heat transfer coefficient (h_{total}) at 1.10 metres and 0.6 metres

14   was calculated with the following:

15     $h_{total} = \beta \left(T_s - T_{op}\right)^{0.1}$ Equation 9

16

17   Where $\beta = 7.67$ (at a distance of 1.1m) and $\beta = 8.21$ (at a distance of 0.6 m) from the slabs.

18   Through calculations of the total heat flux densities (h_{total} and q_{total}) emitted from the floor slabs

19   ranging from temperatures of 30-60 °C with intervals of 5 °C for mean computations. This

20   analysis took into account the basis of thermal energy transfer and enthalpic fluxes supplied

21   from the RFHS.

22

1

2 5.4.1 Heat transfer parameter analysis

3 The thermal characteristics and heat transfer parameters are presented in Figures 16 and 17

4 respectively. On the basis of the heat transfer coefficients and procedures of determination it

5 was noticed that the computed values of the heat transfer coefficients from the Steel Mix (SM)

6 slab RFHS versus the Normal Mix (NM) RFHS were periodically higher for both distances of

7 1.10 m and 0.60 m. As shown in Figure 16, the total heat transfer coefficient (h_{total}) varied

8 from 8.6 W/m^{2}K (at 30 ^{o}C) to 11.7 W/m^{2}K (at 60 ^{o}C) for the NM slab and 9.3 W/m^{2}K (at 30

9 ^{o}C) to 12.2 W/m^{2}K at a distance of 0.6m. Similar heat transfer coefficients were observed for

10 the computed room distance of 1.1 m from the slab. These values are a good estimation in

11 comparison to heat transfer coefficient values obtained in previous studies by Karadağ, 2009;

12 Fontan, 2011 and Cholewa et al. 2013. The study demonstrates a small and minor differences

13 in these heating coefficient values, derived from the temperature differentials (equations 5 and

14 6) when the system is supplied with a higher temperature range of around 55-60 ^{o}C.

15
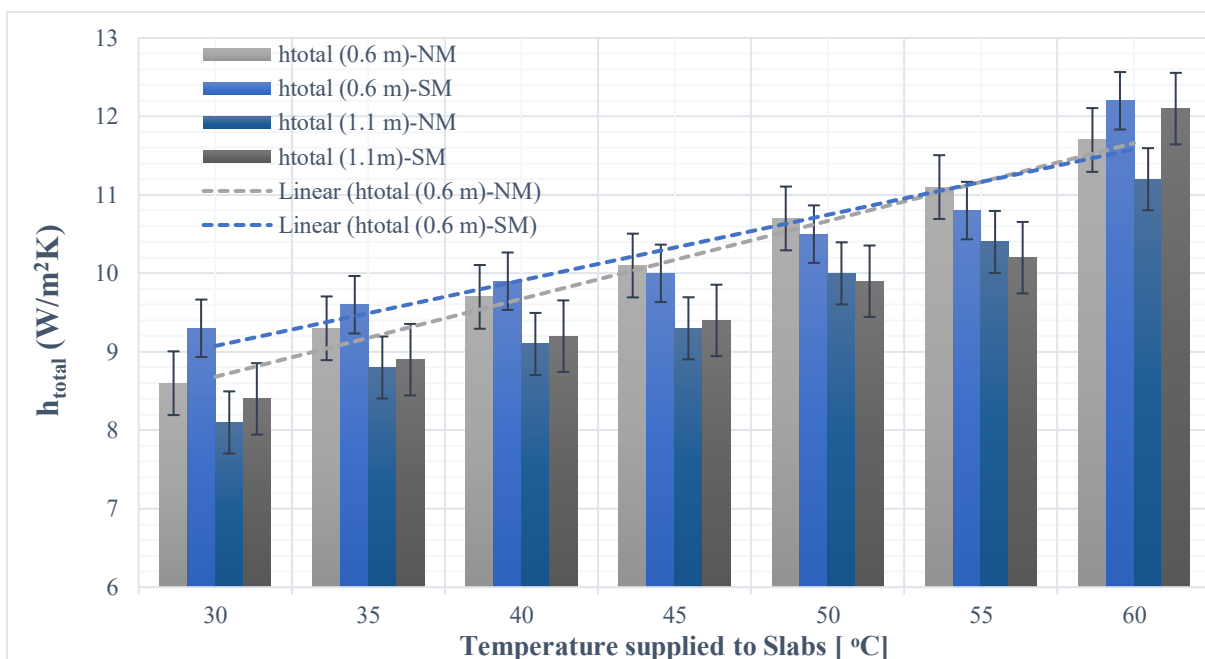
Figure 16: Measured and computed characteristics of the total heat transfer coefficient (h_{total})
2 (W/m^{2}K) for Normal Mix (NM) and Steel Mix (SM) at 0.6 metres and 1.1 metres distances in the
3 room. Temperature Range of 30-60 ^{o}C with intervals of 5 ^{o}C

4

5 **Figure 17**: Measured and computed characteristics of the total heat flux density (q_{total}) (W/m) for
6 Normal Mix (NM) and Steel Mix (SM) at 0.6 metres and 1.1 metres distances in the room.
7 Temperature Range of 30-60 ^{o}C with intervals of 5 ^{o}C

8

9 Heat transfer coefficients are important parameters which dictates energy consumption, cost

10 and thermal comfort and discomfort at various stages. Figure 17 illustrated the continuous but

11 minor gap in the overall total heat flux density (q_{total}) for the NM and SM RFHS. The q_{total} is

12 a very important and fundamental characteristic parameter for radiant floors as a heat transfer

13 parameter. Analysing the data presented, it was noticed that the computed q_{total} of heat transfer

14 are similar to those reported in the literature (Olesen and Zöllner, 2007; Hajabdollahi et al.

15 2012; Zhang et al. 2012; Cholewa et al. 2013) especially for lower temperature ranges for

16 RFHS. The value of the radiant heat transfer coefficients for the heating cycle (between 30-60

17 ^{o}C) is different because of the heating mode and the mechanisms of heat transfer when

18 comparing the NM to SM. The temperature variations and calculations used for the heat

transfer parameters and thermal coefficients were not impacted due to the control mechanisms of the ambient room temperature.

6.0   Conclusions

The experimental measurement and analysis on the overall performance showed that the energy efficiency and thermal performance of RFHS has been implemented and validated with the results presented, which provided some interesting hypotheses for both slab configurations. Both systems showed good responsiveness to intermitted heating operation, achieving uniform floor surface temperatures. The analysis of overlaid graphical plots provided promising results, potentially demonstrating variable energy efficiencies and thermal conductivities of the concrete for the SM and NM. Nevertheless, considering the infrared images and data outputs as well as the SM's reduced capabilities to store thermal energy and a rise in water temperatures being considerably slower for the SM impacted its energetic performance when compared to the NM concrete slab. The SM spreads the heat throughout the slab at a much quicker thermal conductivity rate. As the same heating input is put in across a larger volume, the thermocouples show the temperatures in the SM slab are lower. However, it is expected that the average surface temperature over the entire SM slab would be higher, resulting in a greater heat transfer from the slab to the air. It would be beneficial for test to be further investigated in the field and real-case scenarios to confirm the overall optimum performance of the RFHS infrastructure. In addition, future research can include cube analysis and crushing test with variations in the proportion of steel fine replacements used in the concrete mix. Further research is needed in correlating RFHS infrastructure, life cycle assessment (LCA) and life cycle cost (LCC). The

results of this study could offer supportive information to engineers and manufacturers on the design and use of RFHS.

Conflict of interest

None

References

BS EN 197-1:2011. Cement. *Part 1: Composition, specifications and conformity criteria for common cements.* BSI Standards Limited.

BS EN 12620:2002+A1:2008. Aggregates for concrete. BSI Standards Limited.

AVERYANOVA, M., CICALA, E., BERTRAND, P. & GREVEY, D. 2012. Experimental design approach to optimise selective laser melting of martensitic 17-4 PH powder: part I – single laser tracks and first layer. *Rapid Prototyping Journal,* 18**,** 28-37.

BAEHR, H. D. & STEPHAN, K. 2011. Convective heat and mass transfer. Flows with phase change. *Heat and Mass Transfer.* 3 ed. Germany: Springer-Verlag Berlin Heidelberg.

CHO, J., PARK, B. & LIM, T. 2019. Experimental and numerical study on the application of low-temperature radiant floor heating system with capillary tube: Thermal performance analysis. *Applied Thermal Engineering,* 163.

CHOLEWA, T., ROSIŃSKI, M., SPIK, Z., DUDZIŃSKA, M.R. AND SIUTA-OLCHA, A., 2013. On the heat transfer coefficients between heated/cooled radiant floor and room. *Energy and Buildings*, 66, pp.599-606.

COOK, D., J. & UHER, C. 1974. The thermal conductivity of fibre-reinforced concrete. *Cement and Concrete Research,* 4**,** 497-509.

DAS, S. 2010. *Fundamentals of Heat and Mass Transfer*. Oxford, UK.: Alpha Science International

DEPARTMENT FOR BUSINESS, E. A. I. S. 2019. *Heat in Buildings* [Online]. Available: https://www.gov.uk/government/groups/heat-in-buildings#government-priorities [Accessed 19/02 2020].

FONTANA, L. 2017. Numerical and experimental investigation on a concrete slab thermal conductivity increase due to metal cylinders perpendicular to the slab surface insertion. *Applied Thermal Engineering,* 120**,** 416-430.

FONTANA, L. 2011. Thermal performance of radiant heating floors in furnished enclosed spaces. *Applied Thermal Engineering*, 31(10), pp.1547-1555.

HAJABDOLLAHI, F., HAJABDOLLAHI, Z. AND HAJABDOLLAHI, H., 2012. Thermo-economic modeling and optimization of underfloor heating using evolutionary algorithms. *Energy and Buildings*, 47, pp.91-97.

HAMMOND, P. 13 March 2019. *RE: Spring Statement*

IMIX CONCRETE. 2022. Type C35 / ST4 Concrete | iMix Concrete. [Online]. Available: <https://imixconcrete.co.uk/concrete-strengths-and-grades/type-c35-st4/> [Accessed 17/03/2022].

JOBLI, M., I.,, YAO, R., LUO, Z., SHAHRESTANI, M., LI, N. & LIU, H. 2019. Numerical and experimental studies of a Capillary-Tube embedded PCM component for improving indoor thermal environment. *Applied Thermal Engineering* 148**,** 466-477.

KARADAĞ, R., 2009. The investigation of relation between radiative and convective heat transfer coefficients at the ceiling in a cooled ceiling room. *Energy conversion and management*, 50(1), pp.1-5.

KARAPATIS, N., EGGER, G., GYGAX, P. & GLARDON, R. 1999. Optimisation of powder layer density in selective laser sintering. *Lausanne: Swiss Federal Institute of Technology. Energy Procedia,* 78**,** 2742-2747.

LEVY, S. 2012. *Construction calculations manual*. Waltham, MA: Butterworth-Heinemann, p.234.

MAXILEAD-METALS. 2019. *A Year in Review: 2018's Scrap Metal Recycling Statistics* [Online]. Available: https://maxileadmetals.co.uk/metal-recycling-statistics/ [Accessed 19/02 2020].

MIRIEL, J., SERRES, L. & TROMBE, A. 2002. Radiant ceiling panel heating-cooling systems: experimental and simulated study of the performances, thermal comfort and energy consumptions. *Applied Thermal Engineering,* 22**,** 1861-1873.

OLESEN, B.W. AND ZÖLLNER, G., 2007, June. New European standards for design, dimensioning and testing embedded radiant heating and cooling systems. *In Proceedings of CLIMA* (Vol. 2007).

RENISHAW, P. 2017. Maraging Steel M300 powder for additive manufacturing. *In:* STAFFORDSHIRE (ed.).

RENISHAW PLC 2017. Maraging Steel M300 powder for additive manufacturing. Staffordshire, UK.

ROMANI, J., PEREZ, G. & GRACIA, A. 2017. Experimental evaluation of a heating radiant wall couples to a ground source heat pump. *Renewable Energy,* 105**,** 520-529.

SAMINDA, S., SAMAREKOON, M., RUBEN, P., PEDERSON, J. & EVANGELISTA, L. 2019. Mechanical Performance of Concrete made of steel fibers from tire waste. *Case Studies in Construction Materials,* 11.

SATTARI, S. & FARHANIEH, B. 2006. A parametric study on radiant floor heating system performance. *Renewable Energy,* 31**,** 1617-1626.

TINKER, J., A., & CABRERA, J., G. Modeling the thermal conductivity of concrete based on its measured density and porosity. Building V, 1992. 91-95.

TOFAIL, S., KOUMOULOS, E., BANDYOPADHYAY, A., BOSE, S., O'DONOGHUE, L. & CHARITIDIS, C. 2018. Additive Manufacturing: scientific and technological challenges, market uptake and opportunities. *Materials Today,* 21**,** 22-37.

ZHANG, L., LIU, X.H. AND JIANG, Y., 2012. Simplified calculation for cooling/heating capacity, surface temperature distribution of radiant floor. *Energy and Buildings*, 55, pp.397-404.

ZHENG, W., LUO, B. AND WANG, Y., 2013. Compressive and tensile properties of reactive powder concrete with steel fibres at elevated temperatures. *Construction and Building Materials*, 41, pp.844-851.